^{13}C NMR study of commensurate antiferromagnetism in (TMTTF)$_2$Br

Shinji Hirose,* Yang Liu, and Atsushi Kawamoto†
Department of Condensed Matter Physics, Hokkaido University, Kita-ku, Sapporo, Hokkaido 060-0810, Japan
(Received 30 April 2013; revised manuscript received 5 July 2013; published 12 September 2013)

Quasi-one-dimensional organic conductors (TMT*C*F)$_2X$ have various electric and magnetic properties. Although theoretical and experimental studies have suggested that (TMTTF)$_2$Br has the properties of commensurate antiferromagnetism, details of the magnetic structure of this compound are unclear. Two types of antiferromagnetism are expected, one due to a localized electron and the other to the nesting of the Fermi surface. We therefore assessed the antiferromagnetic structure of (TMTTF)$_2$Br using ^{13}C NMR. Site assignment of the observed antiferromagnetic spectrum confirmed that there were two magnetic molecular sites, with staggered moments and amplitude of $0.11\mu_B$/molecule, as well as nonmagnetic molecular sites. A commensurate structure with antiferromagnetic ordering of ($\uparrow \circ \downarrow \circ$) along a one-dimensional chain would be expected as the freezing of antiferromagnetic fluctuations in the charge-ordered phase of the (TMTTF)$_2$AsF$_6$ salt. The presence of a nodal site is strongly suggestive of the nesting type antiferromagnetism. The fine structure of the antiferromagnetic spectrum suggests superlattice along the interchain direction. We could not observe line broadening due to the charge order above the antiferromagnetic transition.

DOI: 10.1103/PhysRevB.88.125121 PACS number(s): 75.50.Ee, 75.30.Fv, 76.60.−k

I. INTRODUCTION

The organic conductors (TMT*C*F)$_2X$ (C = S; TMTTF: tetramethyltetrathiafulvalene, C = Se; TMTSF: tetramethyltetraselenafulvalene) show various electronic ground states such as charge order (CO), spin density wave (SDW), superconductivity, and antiferromagnetism. Their crystal structures are composed of the donor molecules TMTTF or TMTSF, which stack and are separated by layers of counterions, X [Fig. 1(a)]. The donor molecules stack along the a axis and interact weakly along the b axis. Therefore, (TMT*C*F)$_2X$ are recognized as quasi-one-dimensional conductors. The electronic properties of (TMT*C*F)$_2X$ can be controlled by substituting the counterion X or by applying pressure and can be systematically investigated in connection with a P-T phase diagram [Fig. 1(c)].[1] The compound (TMTSF)$_2$PF$_6$ is the first organic superconductor, with superconductivity emerging at $T_c \leqslant 1.2$ K and at pressures above 0.6 GPa,[2,3] with the incommensurate SDW occurring below 13 K at ambient pressure.[4–7] In (TMTSF)$_2$ClO$_4$, the superconductivity emerges at 1.2 K at ambient pressure.[8] Determination of charge order is also needed to understand the electronic properties of the (TMT*C*F)$_2X$ system. The salts of (TMTTF)$_2$AsF$_6$ and (TMTTF)$_2$SbF$_6$ show CO states below 100 and 157 K, respectively, as well as being in a nonmagnetic insulating state and an antiferromagnetic state, respectively, at low temperature.[9–11] The charge imbalance in the disproportionation state of (TMTTF)$_2$AsF$_6$, $\Delta\rho = \rho_{\mathrm{rich}} - \rho_{\mathrm{poor}}$, was estimated to be $0.16e$ by infrared spectroscopy.[12] We suggested a commensurate antiferromagnetic fluctuation in the CO paramagnetic state of (TMTTF)$_2$AsF$_6$ from NMR study. We recently determined the magnetic structure of the antiferromagnetic phase (AF-I) of (TMTTF)$_2$SbF$_6$,[13] which is on the lower pressure side of (TMTTF)$_2$AsF$_6$. The antiferromagnetic structure of (TMTTF)$_2$SbF$_6$ could be interpreted as a simple up-down moment, which was different from that expected from the fluctuation of the salt (TMTTF)$_2$AsF$_6$.

(TMTTF)$_2$Br is on the high pressure side of (TMTTF)$_2$AsF$_6$. The salt of (TMTTF)$_2$Br shows commensurate antiferromagnetism (AF-II) below 13 K at ambient pressure, with the $b' = c^* \times a$ axis being the easy axis and the a axis being the hard axis.[6,14] Carbon-13 NMR, revealing a four-peak-split antiferromagnetic spectrum, suggested the commensurability of magnetic structure in the salt (TMTTF)$_2$Br. Gap behavior was observed in the spin-lattice relaxation time T_1 of ^{13}C NMR. Under pressure, electric resistivity detected a leap anomaly, suggesting the SDW transition.[15,16] The spin-lattice relaxation time in ^{1}H NMR showed a gapless behavior below the SDW transition temperature and showed a subphase anomaly at 4 K, as in (TMTSF)$_2$PF$_6$,[17] suggesting the incommensurate SDW had become stabilized at high pressure above 0.50 GPa.[16]

Although (TMTTF)$_2$Br has been assessed by NMR, including under high pressure, the structure of the commensurate antiferromagnetism in (TMTTF)$_2$Br has never been clarified. The commensurate antiferromagnetism (AF-II) of (TMTTF)$_2$Br, which is separated from AF-I by the nonmagnetic spin Peierls (SP) state, is thought to be important for understanding P-T phase diagrams of (TMTTF)$_2X$. ^{13}C NMR provides microscopic information about the magnetic state around nuclei. However, conventional ^{13}C NMR with double-sided ^{13}C-enriched molecules involves the Pake doublet problem or restriction of the field direction setting.[18] Therefore, we performed ^{13}C NMR with a one-sided ^{13}C-enriched molecule to determinate the commensurate antiferromagnetic structure of (TMTTF)$_2$Br and to verify the CO state above the antiferromagnetic phase.

II. EXPERIMENT

Single crystals for NMR measurements were prepared electrochemically from one-sided ^{13}C-enriched TMTTF and n-tetrabutylammonium bromide in acetonitrile. One-sided ^{13}C-enriched TMTTF [Fig. 1(b)] was synthesized by coupling the dibutyltin complexes and was prepared as described.[18,19] The advantages of this method include the availability of ^{13}C-dichloroacetic acid methyl ester and the establishment of the precursors of butyltin and ester complexes.[18,20]

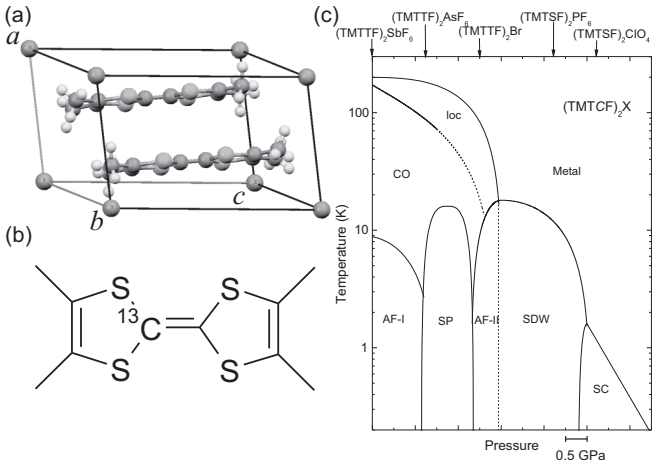

FIG. 1. (a) Crystal structure of $(TMTTF)_2Br$. (b) Molecular structure of one-sided ^{13}C-enriched TMTTF. (c) Pressure-temperature phase diagram of $(TMTCF)_2X$.

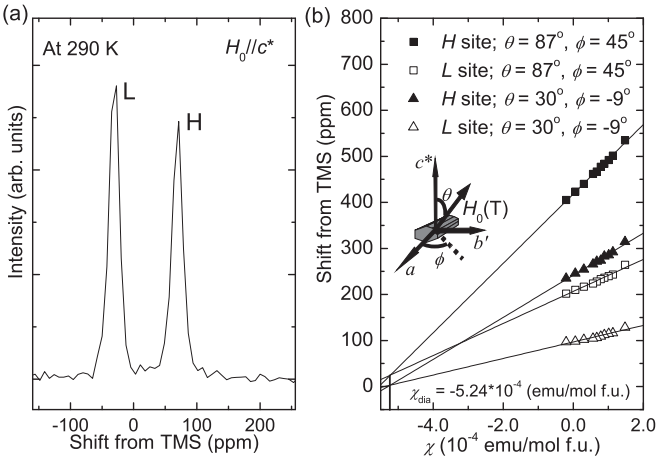

FIG. 2. (a) NMR spectrum of $(TMTTF)_2Br$ at room temperature. (b) Results of δ-χ plots at two local nuclear sites, H and L (Ref. 21).

One-sided ^{13}C-enriched TMTTF eliminates spectral splitting by Pake doublets and enables easy analysis of NMR spectra. Crystal orientation was determined by x-ray diffraction. NMR experiments were performed in a magnetic field of 9.4 T, and NMR spectra were obtained by fast Fourier transformation of the spin echo with a $\pi/2$-π pulse sequence. The typical $\pi/2$ pulse width was 4 μs. The spin-lattice relaxation time was determined by the saturation recovery method.

III. RESULTS AND DISCUSSION

A. Determination of hyperfine coupling and chemical shift tensors

Figure 2(a) shows the NMR spectrum of $(TMTTF)_2Br$ at 290 K. Two peaks from two crystallographically independent ^{13}C nuclei were observed and were assigned to the two central C=C carbon sites, H and L. The NMR shift at a local nuclear site can be expressed as the sum of the Knight shift K and the chemical shift σ as $\delta = K + \sigma = a\chi_s + \sigma$. The Knight shift can be expressed as the product of the hyperfine coupling constant a and the spin susceptibility χ_s. Spin susceptibility can also be expressed as $\chi_s = \chi - \chi_{\rm dia}$, where χ and $\chi_{\rm dia}$ are the static susceptibility and diamagnetic susceptibility, respectively. In the π-orbital system, due to the anisotropic contribution of the π orbital, the hyperfine coupling constant a and the chemical shift σ depend on the direction of the magnetic field and can be expressed as

$$a = \tilde{\mathbf{h}}\mathbf{A}\mathbf{h}, \quad \sigma = \tilde{\mathbf{h}}\boldsymbol{\sigma}\mathbf{h}. \tag{1}$$

Here, $\mathbf{h}$ is the directional cosine of the magnetic field; $\mathbf{A}$ and $\boldsymbol{\sigma}$ are the hyperfine coupling and chemical shift tensors, respectively; and the Knight shift corresponds to the diagonal components of the hyperfine coupling tensor. By contrast, in the antiferromagnetic state, the NMR shift is due to the local field induced by the ordered moment. As the local field couples with the moment via the off-diagonal component of the tensor, the hyperfine coupling tensors are necessary to estimate the size of the ordered moment. We therefore evaluated both the hyperfine coupling and chemical shift tensors at several angles from the δ-χ plot shown in Fig. 2(b). The δ-χ plot at each angle follows the relational formula $\delta_i = a_i(\chi - \chi_{\rm dia}) + \sigma$, where the subscript i denotes the local nuclear sites H and L. The hyperfine coupling constant, which depends on the crystallographically independent local nuclear site on the molecule, can be obtained from the slope of the δ-χ plot. In contrast, the chemical shift is caused by the shielding field from the coherent orbital current and is not sensitive to the site in the molecule. Therefore, the chemical shift can be obtained by the intersection of the δ-χ plots at two local nuclear sites. To determine the hyperfine coupling constant a and chemical shift σ we measured the temperature dependence of the NMR shift at these two local sites at several angles.[22] As the intersection of lines at H and L sites corresponds to $\chi_s = 0$, the diamagnetic susceptibility was estimated as -5.24×10^{-4} emu/mol f.u. Using Eq. (1), the hyperfine coupling and chemical shift tensors were calculated as

$$\mathbf{A}_{\rm H} = \begin{pmatrix} A_{aa} & A_{ab'} & A_{ac^*} \\ A_{ab'} & A_{b'b'} & A_{b'c^*} \\ A_{ac^*} & A_{b'c^*} & A_{c^*c^*} \end{pmatrix}_{\rm H} = \begin{pmatrix} 8.07(7) & 0.29(8) & 0.43(8) \\ 0.29(8) & -0.3(1) & 0.03(8) \\ 0.43(8) & 0.03(8) & 0.06(8) \end{pmatrix} ({\rm kOe}/\mu_B), \tag{2}$$

$$\mathbf{A}_{\rm L} = \begin{pmatrix} A_{aa} & A_{ab'} & A_{ac^*} \\ A_{ab'} & A_{b'b'} & A_{b'c^*} \\ A_{ac^*} & A_{b'c^*} & A_{c^*c^*} \end{pmatrix}_{\rm L} = \begin{pmatrix} 4.93(6) & 0.06(7) & 0.30(7) \\ 0.06(7) & -1.36(8) & 0.04(7) \\ 0.30(7) & 0.04(7) & -0.77(8) \end{pmatrix} ({\rm kOe}/\mu_B), \tag{3}$$

$$\boldsymbol{\sigma} = \begin{pmatrix} \sigma_{aa} & \sigma_{ab'} & \sigma_{ac^*} \\ \sigma_{ab'} & \sigma_{b'b'} & \sigma_{b'c^*} \\ \sigma_{ac^*} & \sigma_{b'c^*} & \sigma_{c^*c^*} \end{pmatrix} = \begin{pmatrix} -42(6) & 8(7) & -28(7) \\ 8(7) & 124(9) & -9(8) \\ -28(7) & -9(8) & 63(7) \end{pmatrix} ({\rm ppm}). \tag{4}$$

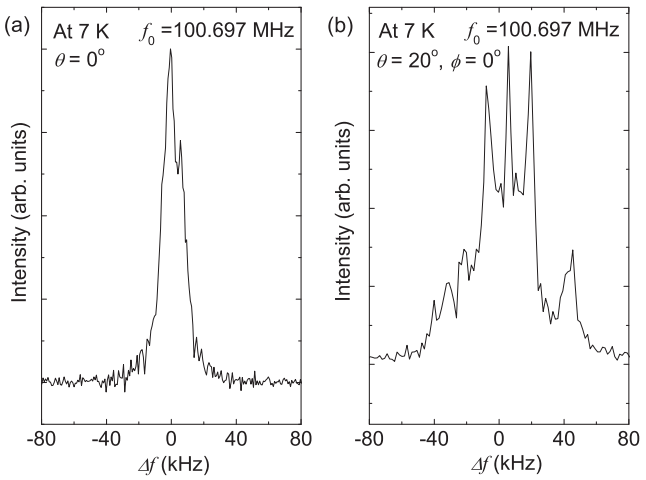

FIG. 3. Antiferromagnetic spectra at 7 K. A magnetic field was applied at angles of $\theta = 0^{\circ}$ and $\theta = 20^{\circ}$, $\phi = 0^{\circ}$ in the ac^* plane. Here θ and ϕ correspond to the field conditions in the inset of Fig. 2(b).

As $(TMTCF)_2X$ has an isomorphic structure, these tensors can be utilized as basic parameters for ^{13}C NMR of $(TMTTF)_2X$ and are consistent with those of $(TMTSF)_2PF_6$.[20]

B. Examination of antiferromagnetic structure

By evaluating the hyperfine coupling tensors, we could assess the commensurate antiferromagnetic spectrum. To prevent spin flop, the magnetic field should be applied perpendicular to the easy axis. In this case, we could observe the moment via an off-diagonal element of the hyperfine coupling tensor. However, in a field parallel to the c^* axis, the moment makes an internal field via the small hyperfine coupling of $A_{b'c^*}$. Indeed, as shown in Fig. 3(a), we observed a broadened low resolution spectrum in the antiferromagnetic state in this setting. By considering the spectrum width of one NMR pulse and the amplitude of the hyperfine coupling constants, we measured the NMR spectrum by applying a magnetic field along the tilted angle $\theta = 20^{\circ}$, $\phi = 0^{\circ}$ ([Fig. 2(b), inset]. Figure 3(b) shows that the NMR spectrum at this setting consists of approximately five peaks at around $\Delta f = 45$, 20, 5, -10, and -25 kHz (doublet), suggesting a commensurate structure. To assign the antiferromagnetic spectrum, we calculated the hyperfine coupling tensors in this setting as

$$\mathbf{A}_{\mathrm{H}} = \begin{pmatrix} A_{kk} & A_{kb'} & A_{kh} \\ A_{kb'} & A_{b'b'} & A_{b'h} \\ A_{kh} & A_{b'h} & A_{hh} \end{pmatrix}_{\mathrm{H}} = \begin{pmatrix} 6.81(5) & 0.25(5) & 3.01(6) \\ 0.25(5) & -0.3(1) & 0.12(5) \\ 3.01(6) & 0.12(5) & 1.34(5) \end{pmatrix} (\mathrm{kOe}/\mu_{\mathrm{B}}), \quad (5)$$

$$\mathbf{A}_{\mathrm{L}} = \begin{pmatrix} A_{kk} & A_{kb'} & A_{kh} \\ A_{kb'} & A_{b'b'} & A_{b'h} \\ A_{kh} & A_{b'h} & A_{hh} \end{pmatrix}_{\mathrm{L}} = \begin{pmatrix} 4.06(4) & 0.03(4) & 2.17(6) \\ 0.03(4) & -1.36(8) & 0.06(4) \\ 2.17(6) & 0.06(4) & 0.15(4) \end{pmatrix} (\mathrm{kOe}/\mu_{\mathrm{B}}). \quad (6)$$

Here, the h axis denotes the magnetic field direction and the k axis is perpendicular to the b' and h axes. The internal field along the h axis induced by the moment is proportional to the $A_{b'h}$ component of the hyperfine coupling tensor. Since the ratio of hyperfine coupling components at the H and L local nuclear sites is 2:1, the peaks at around $\Delta f = 45$ and 20 kHz could be assigned to the H and L nuclear sites, respectively, on molecules with moments parallel to the b' axis, and the peaks at around $\Delta f = -10$ and -25 kHz could be assigned to the L and H nuclear sites, respectively, on the molecules with moments antiparallel to the b' axis. In addition, the peak at around $\Delta f = 5$ kHz was observed at the chemical shift position and could be assigned to the H and L nuclear sites on the nonmagnetic molecular site. From the split widths at the H and L nuclear sites on the molecules with parallel and antiparallel moments, the internal fields at these nuclear sites were estimated at 70 and 30 Oe, respectively. Using a hyperfine coupling constant of $A_{b'h}$, the size of the ordered moment was estimated at $0.11\mu_B$/molecule.

C. Spin-lattice relaxation time at commensurate antiferromagnetism

To examine the peaks of the nonmagnetic molecules in detail and to confirm the site assignments, we measured the temperature dependence of the spin-lattice relaxation time. Figure 4(a) shows the temperature dependence of the spin-lattice relaxation rate for the corresponding peaks shown in Fig. 4(b). The open inverted triangles and triangles correspond to the peaks at around $\Delta f = -33$ and 43 kHz, respectively, both derived from the L-nuclear sites on the magnetic molecule. The filled inverted triangles, diamonds, and triangles correspond to the peaks at $\Delta f = -93$, 92, and 102 kHz, respectively, derived from the H-nuclear site on the

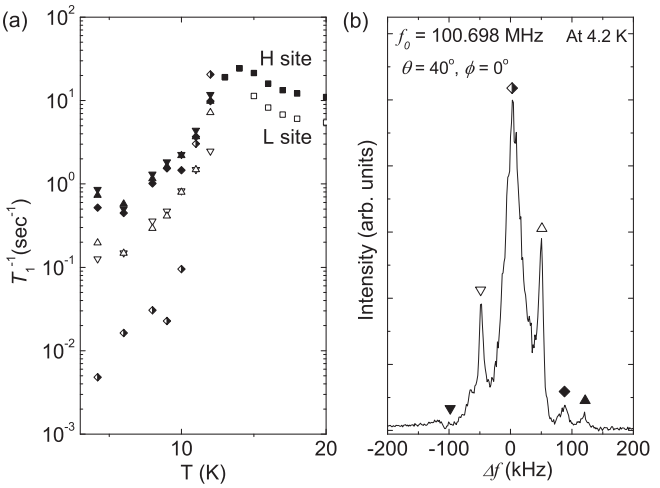

FIG. 4. (a) Spin-lattice relaxation rate of NMR signals shown in Fig. 4(b). The open inverted triangles and triangles correspond to peaks at around $\Delta f = -33$ and 43 kHz, respectively, the filled inverted triangles, diamonds, and triangles correspond to peaks at $\Delta f = -93$, 92, and 102 kHz, respectively, and the half-filled diamonds correspond to a peak at around $\Delta f = 4$ kHz. (b) Antiferromagnetic spectrum at 4.2 K. A magnetic field was applied in the ac^* plane. Here θ and ϕ correspond to the angle shown in Fig. 2(b), inset, as detailed field conditions.

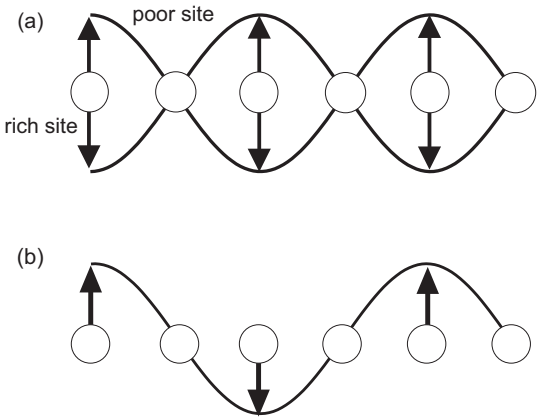

FIG. 5. (a) Schematic of the commensurate antiferromagnetic fluctuation of $(TMTTF)_2AsF_6$.[12] (b) Schematic of the commensurate antiferromagnetic structure predicted for $(TMTTF)_2Br$.

magnetic molecule. The spin-lattice relaxation rate of the peak at around $\Delta f = 4$ kHz is represented by half-filled diamonds and corresponds to the nonmagnetic molecule. The spin-lattice relaxation rate on magnetic molecules showed thermal activation behavior, consistent with previous ^{13}C NMR.[6] The sets of the open symbols showed the almost same values and temperature dependence and those of the filled symbols showed the almost same values and temperature dependence, suggesting the validity of the site assignment. The spin-lattice relaxation rate at the nonmagnetic sites showed similar thermal activation behavior. Although sufficient recovery time is needed to observe the central peak, the peak intensity of the nonmagnetic molecule was comparable to that at other magnetic sites without sample or batch dependence. Therefore, the nonmagnetic site is considered intrinsic.

D. Magnetic structure of the commensurate antiferromagnetic phase

The site assignment of the antiferromagnetic spectra suggested that there are three independent molecules in the commensurate antiferromagnetic phase of the salt $(TMTTF)_2Br$ (AF-II). We first considered magnetic correlation along the direction of molecular stacking. As shown in Fig. 1(c), the AF-II phase of $(TMTTF)_2Br$ is adjacent to the CO phase of $(TMTTF)_2AsF_6$, suggesting a close relationship between the magnetic fluctuation in $(TMTTF)_2AsF_6$ and the static magnetic structure of $(TMTTF)_2Br$. Previously, the different temperature dependencies of the spin-lattice relaxation rate between charge-rich and charge-poor sites suggested a commensurate antiferromagnetic fluctuation in the CO state of $(TMTTF)_2AsF_6$ [Fig. 5(a)], in which nodes are located at charge-poor molecules and antinodes at charge-rich molecules.[12] The alternative arrangement, rich-poor-rich-poor, in the CO state was confirmed by finding the second harmonic generation (SHG) in the absence of the lattice doubling.[23] In the case of the commensurate SDW, the antiferromagnetic fluctuation of the AsF_6 predicted the sinusoidal wave modulation. Freezing of the commensurate antiferromagnetic fluctuation should yield a magnetic structure in the AF-II phase [Fig. 5(b)].

Two types of antiferromagnetism have been expected: the antiferromagnetism of localized spin and SDW antiferromagnetism due to the nesting instability of the Fermi surface. In the case of the antiferromagnetism of the localized spin, the nonmagnetic molecules cannot be explained. Although the fitting of the angular dependence of the NMR shift was analyzed by assuming a nesting vector of (0.5,0.25,*), in ^{1}H NMR,[24] to confirm whether antiferromagnetism was due to the localized spin or the nesting of the Fermi surface, experimental evidence for nodal structure as shown in Fig. 5(b) is required. The antiferromagnetic structure shown in Fig. 5(b) results in a 1:1 ratio of node to antinode molecules. Node sites correspond to the nonmagnetic sites and antinode sites correspond to magnetic sites in Fig. 4(b). Since the central peak consists of peaks of the H and L nuclear sites, the intensity ratio of peaks at $\Delta f = -33$, 4, and 43 kHz is expected to be 1:4:1. Indeed, the sufficiently recovered spectrum showed an approximate ratio of 1:4:1, consistent with the freezing structure shown in Fig. 5(b). A recent ^{13}C-NMR study suggested an antiferromagnetic structure with a charge order of $([\Uparrow - \uparrow] - [\Downarrow - \downarrow])$ in the antiferromagnetic phase of the $(TMTTF)_2SbF_6$ salt (AF-I), in which $\Uparrow$ and $\Downarrow$ denote the staggered moments at charge-rich sites, $\uparrow$ and $\downarrow$ denote the staggered moments at charge-poor sites, and [ ] denotes TMTTF dimers. This means that the magnetic structure of the AF-I phase is qualitatively different from the structure observed in the AF-II phase.[13]

We next focused on the magnetic structure along the inter-column direction. In the fine structure of the spectrum, a doublet was observed at the peak of the magnetic molecules. For example, split peaks were observed around $\Delta f = -25$ kHz at a field condition of $\theta = 20^o$ [Fig. 3(b)] and around $\Delta f = 102$ kHz at a field condition of $\theta = 40^o$ [Fig. 4(b)]. We also observed splitting of the L-site peak in the other setting. Assuming a basic structure in Fig. 5(b), which is formed along the molecular stacking column, this splitting suggests two crystallographically independent columns. $(TMTCF)_2X$ salts have a warped one-dimensional Fermi surface with a nesting vector approximately equal to (0.5,0.25,0). The magnetic structure along the molecular stacking column corresponds to the vector of $0.5\boldsymbol{a}^*$. The double column structure with nodal molecules could explain the superlattice structure with the vector of $0.25\boldsymbol{b}^*$ as shown in Fig. 6. The crystallographically independent stacking columns A and B detect different dipole fields, resulting in the slightly doublet spectrum observed in Figs. 3(b) and 4(b). The gapless behavior of T_1 and the anomaly of T_1 at lower temperature and under pressure suggested the existence of a subphase in $(TMTTF)_2Br$, similar to that in the incommensurate SDW of $(TMTSF)_2PF_6$.[15] Incommensurate SDW is suggested at the high pressure side of the AF-II phase. Since the SDW phase is adjacent to the AF-II phase in the phase diagram, the pressure dependence of the NMR spectrum in our experimental setting with the high resolution is interesting.

E. Charge order and commensurate antiferromagnetism

^{13}C NMR suggested a close relationship between the antiferromagnetic structure of $(TMTTF)_2Br$ and the commensurate antiferromagnetic fluctuation of $(TMTTF)_2AsF_6$. In $(TMTTF)_2AsF_6$, the antinodes and nodes in antiferromagnetic fluctuation are likely located on the charge-rich and

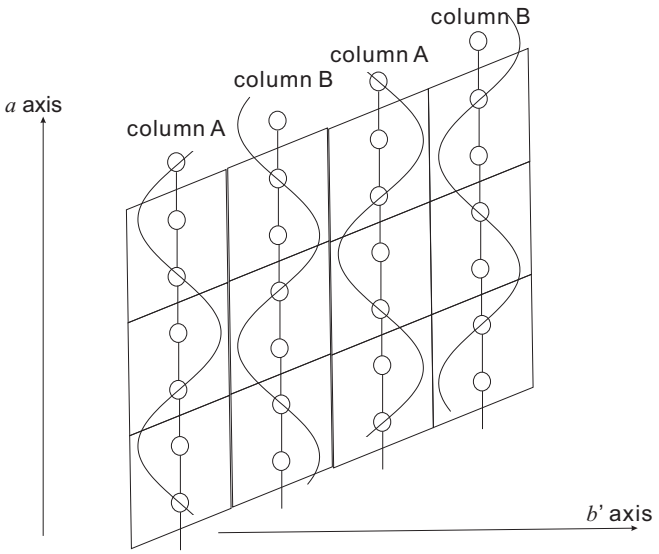

FIG. 6. Schematic of the commensurate antiferromagnetic structure predicted by the NMR results shown in Figs. 3(b) and 4(b).

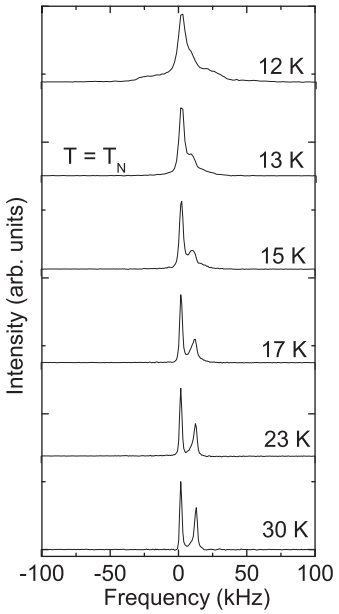

FIG. 7. Temperature dependence of the NMR spectrum corresponding to the field condition shown in Fig. 4(b).

charge-poor sites, respectively. Therefore, a charge anomaly above T_N is expected for $(TMTTF)_2Br$. Indeed, previous ^{13}C-NMR measurements showed a broadening of the inhomogeneous width around 18 K, suggesting a charge-ordered phase.[25] We therefore examined this anomaly in our experimental settings. Figure 7 shows the temperature dependence of NMR spectra at the same angle as in Fig. 4(b). At low temperatures below 13 K, antiferromagnetic spectra were observed, whereas broadening of the linewidth by charge order was not clearly observed at 18 K. Below 17 K, the peak at the H nuclear site, which has a larger coupling constant, showed slight broadening above the antiferromagnetic ordering temperature. When charge order occurs, the peak should split or broaden at any nuclear site due to a chemical shift. Therefore, linewidth broadening only at the H local nuclear site may correspond to a premonitory anomaly, due not to charge order but to the precursor of the antiferromagnetic transition, a finding consistent with the spin-lattice relaxation rate, which increased abruptly below 20 K. Moreover, infrared spectroscopy study shows that the charge imbalances between charge-rich and charge-poor sites were $\Delta\rho = 0.29$, 0.21, and 0.16 and the transition temperatures were $T_{CO} = 150$, 100, and 65 K in the charge-ordered states of $(TMTTF)_2SbF_6$, $(TMTTF)_2AsF_6$, and $(TMTTF)_2PF_6$, respectively.[26] These results suggest that the charge imbalance and the transition temperature decrease as chemical pressure increases. Since $(TMTTF)_2Br$ is located on the high pressure side of $(TMTTF)_2PF_6$, the charge imbalance may become smaller and the transition temperature may drop to the antiferromagnetic transition temperature of $(TMTTF)_2Br$. Thus, an investigation using a nonmagnetic probe is required to determine whether symmetry has been broken. Raman scattering spectroscopy and x-ray diffraction recently suggested a charge-order transition below the antiferromagnetic transition temperature.[27]

IV. CONCLUSION

We performed ^{13}C-NMR measurements of the commensurate antiferromagnetic phase of $(TMTTF)_2Br$ including the temperature dependence of T_1^{-1}. Using these data, we determined the hyperfine coupling and chemical shift tensors of this compound. These tensors can be utilized as basic parameters for $(TMTTF)_2X$ salts. We confirmed that the commensurate antiferromagnetic spectrum showed the size of ordered moment being $0.11\mu_B$/molecule. Since we observed three types of magnetic and nonmagnetic sites, a column structure of $(\uparrow \circ \downarrow \circ)$ could be predicted, which is consistent with the freezing of the fluctuation observed in $(TMTTF)_2AsF_6$. The doublet structure on the magnetic molecules suggested a double column structure along the b' axis and was consistent with the $(0.5,0.25,^*)$ vector. We did not observe line broadening due to charge disproportionation at 18 K, suggesting that the spectral broadening corresponds to the precursor of antiferromagnetic transition.

ACKNOWLEDGMENTS

The authors thank Y. Ihara and N. Matsunaga of Hokkaido University for valuable discussions. This study was supported in part by a Grant-in-Aid for Science Research (Grant No. 24540353) from the Ministry of Education, Culture, Sports, Science and Technology.

*hirose1026@mail.sci.hokudai.ac.jp
†atkawa@phys.sci.hokudai.ac.jp

[1]D. Jérome, Science **252**, 1509 (1991).
[2]D. Jérome, A. Mazaud, M. Ribault, and K. Bechgaard, J. Phys. Lett. **41**, 95 (1980).
[3]T. Vuletić, P. Auban-Senzier, C. Pasquier, S. Tomić, D. Jérome, M. Héritier, and K. Bechgaard, Eur. Phys. J. B **25**, 319 (2002).
[4]T. Takahashi, Y. Maniwa, H. Kawamura, and G. Saito, Physica B+C (Amsterdam) **143**, 417 (1986).

[5]T. Takahashi, Y. Maniwa, H. Kawamura, and G. Saito, J. Phys. Soc. Jpn. **55**, 1364 (1986).
[6]E. Barthel, G. Quirion, P. Wzietek, D. Jérome, J. B. Christensen, M. Jørgensen, and K. Bechgaard, Europhys. Lett. **21**, 87 (1993).
[7]S. Valfells, P. Kuhns, A. Kleinhammes, J. S. Brooks, W. Moulton, S. Takasaki, J. Yamada, and H. Anzai, Phys. Rev. B **56**, 2585 (1997).
[8]K. Bechgaard, K. Carneiro, M. Olsen, F. B. Rasmussen, and C. S. Jacobsen, Phys. Rev. Lett. **46**, 852 (1981).
[9]W. Yu, F. Zhang, F. Zamborszky, B. Alavi, A. Baur, C. A. Merlic, and S. E. Brown, Phys. Rev. B **70**, 121101(R) (2004).
[10]D. S. Chow, F. Zamborszky, B. Alavi, D. J. Tantillo, A. Baur, C. A. Merlic, and S. E. Brown, Phys. Rev. Lett. **85**, 1698 (2000).
[11]F. Zamborszky, W. Yu, W. Raas, S. E. Brown, B. Alavi, C. A. Merlic, and A. Baur, Phys. Rev. B **66**, 081103(R) (2002).
[12]S. Hirose, A. Kawamoto, N. Matsunaga, K. Nomura, K. Yamamoto, and K. Yakushi, Phys. Rev. B **81**, 205107 (2010).
[13]N. Matsunaga, S. Hirose, N. Shimohara, T. Satoh, T. Isome, M. Yamomoto, Y. Liu, A. Kawamoto, and K. Nomura, Phys. Rev. B **87**, 144415 (2013).
[14]K. Yamaji, J. Phys. Soc. Jpn. **56**, 860 (1986).
[15]B. J. Klemme, S. E. Brown, P. Wzietek, G. Kriza, P. Batail, D. Jerome, and J. M. Fabre, Phys. Rev. Lett. **75**, 2408 (1995).
[16]A. Ishikawa, N. Matsunaga, K. Nomura, T. Sasaki, T. Nakamura, T. Takahashi, and G. Saito, Phys. Rev. B **67**, 212404 (2003).
[17]B. J. Klemme, S. E. Brown, P. Wzietek, D. Jérome, and J. M. Fabre, J. Phys. I France **6**, 1745 (1996).
[18]S. Hirose, M. Misawa, and A. Kawamoto, Crystals **2**, 1034 (2012).
[19]J. Yamada, S. Satoki, S. Mishima, N. Akashi, K. Takahashi, N. Masuda, Y. Nishimoto, S. Takasaki, and H. Anzai, J. Org. Chem. **61**, 3987 (1996).
[20]Y. Kimura, M. Misawa, and A. Kawamoto, Phys. Rev. B **84**, 045123 (2011).
[21]A. Kagiwada, Master's thesis, Hokkaido University, 2004.
[22]See Supplemental Material at http://link.aps.org/supplemental/10.1103/PhysRevB.88.125121 for Table of the hyperfine coupling constants and chemical shifts of $(TMTTF)_2Br$.
[23]K. Yamamoto, A. Kawamoto, N. Matsunaga, K. Nomura, and K. Yakushi, Meeting Abstracts of the Physical Society of Japan **66**, 885 (2011).
[24]T. Nakamura, T. Nobutoki, Y. Kobayashi, T. Takahashi, and G. Saito, Synth. Met. **70**, 1293 (1995).
[25]S. Fujiyawa and T. Nakamura, Synth. Met. **133-134**, 67 (2003).
[26]T. Knoblauch and M. Dressel, Phys. Status Solidi C **9**, 1158 (2012).
[27]R. Kondo, A. Toda, Y. Nogami, A. Nakano, and R. Kumai, Meeting Abstracts of the Physical Society of Japan **68**, 936 (2013).